Atmospheric Environment 309 (2023) 119903

Contents lists available at ScienceDirect

Atmospheric Environment

journal homepage: www.elsevier.com/locate/atmosenv

Understanding the atmospheric transformation mechanism of an emerging fluorinated alcohol (FESOH)

Guochun Lv [a,b], Jiaoxue Yang [c], Xiaomin Sun [d,*], Guiyin Wang [a], Zhang Cheng [a], Zhanbiao Yang [a], Changlian Xu [a], Junzhuo Cai [a], Xiaoxun Xu [a,**]

[a] College of Environmental Sciences, Sichuan Agricultural University, Chengdu, 611130, China
[b] College of Grassland Science and Technology, Sichuan Agricultural University, Chengdu, 611130, China
[c] School of Geography and Environment, Liaocheng University, Liaocheng, 252000, China
[d] Environment Research Institute, Shandong University, Qingdao, 266237, China

HIGHLIGHTS

- Three main conformers of FESOH account for approximate 99% of all conformers.
- The H-abstraction at α-C and β-C mainly occurs for ·OH-initiated FESOH degradation.
- Subsequent reactions can form alkyl peroxynitrite, fluorinated aldehyde and CF_3OH.
- FESOH and its transformation products cannot be accumulated in organisms.

GRAPHICAL ABSTRACT

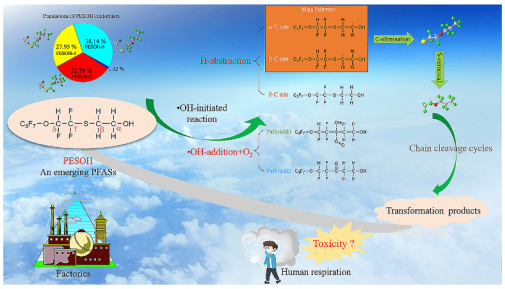

ARTICLE INFO

Keywords:
PFASs
FESOH
Atmospheric transformation
OH radicals
Theoretical calculation

ABSTRACT

One important pathway for human exposure to per- and polyfluorinated alkyl substances (PFASs) is based on the Earth's atmosphere. Figuring out atmospheric transformation mechanism of PFASs is beneficial for understanding their effects on humans. However, the focus on the molecular-level transformation mechanism of emerging PFASs in the atmosphere still need to be improved. In this work, we used quantum chemistry calculation to study ·OH-initiated degradation mechanism of a new fluorinated alcohol ($C_3F_7OCHFCF_2SCH_2CH_2OH$, abbreviated FESOH) in the presence of oxygen and nitric oxide. Three main conformers of FESOH share the similar initial mechanism that the abstraction reactions of H atom at α-C and β-C atoms are the main pathways (activation free energies of <10 kcal mol^{-1} at 298 K), but make different contributions to the whole FESOH degradation. Subsequent transformations starting from initial products at α-C atoms will reunite with that at β-C atoms, and the intermediate ($C_3F_7OCHFCF_2S\cdot$) is produced. After O_2 addition to the intermediate and the following SO_2 elimination, the alkyl radical ($C_3F_7OCHFCF_2\cdot$) can undergo consecutive chain cleavage cycles to form CF_3OH finally. The bioaccumulation evaluation shows that FESOH and its transformation products cannot

* Corresponding author.
** Corresponding author.
E-mail addresses: [redacted]@sdu.edu.cn (X. Sun), [redacted]@sicau.edu.cn (X. Xu).

https://doi.org/10.1016/j.atmosenv.2023.119903
Received 11 March 2023; Received in revised form 30 May 2023; Accepted 12 June 2023
Available online 14 June 2023

be accumulated in organisms. The work is helpful for knowing the atmospheric fate of FESOH at molecular level and can provide some insight into the transformation of other PFASs in the atmosphere.

1. Introduction

As a type of synthetic chemicals, per- and polyfluorinated alkyl substances (PFASs) have been used in many fields such as metal plating (Wang et al., 2013), textile(Wang et al., 2017) and firefighting (Glüge et al., 2020). In their manufacturing, usage and disposal processes, PFASs can be emitted into the environment (Lohmann et al., 2020). They have been widely detected in water (Podder et al., 2021), soil (Chen et al., 2016) and atmosphere (Yu et al., 2018), and have aroused widespread concern due to their persistence, bioaccumulation and toxicity (Liu et al., 2018; Lv and Sun, 2021; Dickman and Aga, 2022; Li et al., 2022). In addition to food intake and water ingestion, air inhalation is also an important pathway for human exposure to PFASs (Harrad et al., 2010; Tansel, 2022), leading scientists to consider the distribution, transportation and transformation of PFASs in the atmosphere so as to evaluate their environment and health impact.

In the atmospheric environment, ionizable PFASs like perfluoroalkyl acids (PFAAs) and neutral PFASs are both found (Yao et al., 2016, 2017). Ionizable PFASs mainly exist in the atmospheric particulate matter (Wang et al., 2020). For neutral PFASs, they can be found in gas phase and aerosols, and most of them can be oxidized by some atmospheric radicals (Wallington et al., 2006) and through photochemical reactions (Styler et al., 2013). The neutral PFASs found in the atmosphere include fluorinated alcohols (Yao et al., 2016), fluorinated sulfonamides (Dreyer et al., 2009), etc.

Fluorinated alcohols are the predominant neutral PFASs in the atmosphere. Fluorotelomer alcohols (FTOHs, $C_nF_{2n+1}CH_2CH_2OH$), one of the main fluorinated alcohols, have been regarded as the potential source of perfluorocarboxylic acids (PFCAs) in remote region, and have the atmospheric lifetime of about 20 days, which is determined by reaction with OH radical (Ellis et al., 2003). The atmospheric oxidation products of FTOHs are mainly PFCAs in the absence of NO_x (Ellis et al., 2004), but no PFCAs occur when NO_x exists (Sulbaek Andersen et al., 2005). Using the atmospheric chemistry model, Wallington et al. (2006) studied the ratio of PFCAs in the transformation products of 8:2 FTOH ($C_8F_{17}CH_2CH_2OH$). Their results show that the molar yield of perfluorooctanoic acid (PFOA) is within the range of 1% and 10% and depends on location and season. The following model studies also illustrated that the atmospheric oxidation of FTOHs is the potential source of atmospheric PFCAs (Yarwood et al., 2007; Thackray and Selin, 2017; Thackray et al., 2020).

Because of wide distribution, persistence, toxicity, and bioaccumulation, PFOA and perfluorooctanesulfonate (PFOS), the two most commonly used PFASs, have been listed in annexes of Stockholm Convention text as POPs. Thus, the production and usage of these PFASs are eliminated and restricted. Considering their enormous marketing demand, alternatives of these PFASs have been designed, produced, and used. As an alternative of the traditional PFASs, a new fluorosurfactant (diFESOS) has been used in the European market (Folkerson et al., 2021). A fluorinated alcohol ($C_3F_7OCHFCF_2SCH_2CH_2OH$, abbreviated FESOH) is the important raw material of the diFESOS (Joudan et al., 2022), and can also be produced from the microbial biotransformation of diFESOS in activated sludge (Joudan and Mabury, 2022) and the rat metabolism of diFESOS (Folkerson et al., 2021). An experiment study has discussed the atmospheric fate of FESOH by analyzing the kinetics and product of the reaction between FESOH with OH radicals (or chlorine atoms) (Joudan et al., 2022). However, the detailed reaction mechanism of FESOH with atmospheric radicals is still unclear. Theoretical calculations can obtain the information of the reaction intermediates and transition states in the reaction processes, thus is an effective tool to study the reaction mechanism.

In this work, we want to use theoretical calculation to study the atmospheric reaction of FESOH with OH radicals in the presence of O_2 and NO. The conformation searching was firstly performed to confirm the most stable conformation of FESOH. The initial rate constants of FESOH by OH radicals at different temperatures were calculated using kinetic analysis. The subsequent reaction processes and the most favorable reaction pathways were also investigated. To evaluate the change of bioaccumulation potential in reaction processes, the bioaccumulation and bioconcentration factors of FESOH and its degradation products were finally evaluated.

2. Methods

2.1. Conformation searching

Because the linear structure of FESOH results in the existence of many conformers, the first thing we need to do is to search the minimum energy conformer. We firstly used Confab module (O'Boyle et al., 2011a, b) in Openbabel program (O'Boyle et al., 2011a,b) to generate 234 initial conformers of FESOH. These initial conformers were pre-optimized by MOPAC 2016 (Stewart, 2016) with the PM7 method (Stewart, 2013), and the isostat module of the Molclus program (Lu, 2021) was used to eliminate the repeated structures and to sort these conformers on the basis of the corresponding energies. The 10 conformers of lower energies were re-optimized using the higher accuracy method B3LYP-D3(BJ)/6–311++g(d,p) so as to obtain the minimum energy conformer.

2.2. DFT calculations

All calculations including the final step of conformation searching were performed using Gaussian 16 software suite (Frisch et al., 2016). The geometric optimization and frequency calculations were carried out using the B3LYP functional (Becke, 1993) with Grimme's D3 dispersion correct (Becke-Johnson damping) (Grimme et al., 2011) and 6–311++g (d,p) basis set (Krishnan et al., 1980; McLean and Chandler, 1980), that is, B3LYP-D3(BJ)/6–311++g(d,p). To ensure that the transition state is connected with the corresponding reactants and products, intrinsic reaction coordinate (IRC) calculation (Fukui, 1981; Hratchian and Schlegel, 2004, 2005) was executed. The single-point energies of these optimized structures were refined using the B2PLYP double hybrid functional (Grimme, 2006) with Grimme's D3 dispersion correct (Becke-Johnson damping) (Grimme et al., 2011) and Def2TZVP basis set (Weigend and Ahlrichs, 2005; Weigend, 2006). The CYLview software package was used to visualize these optimized species (Legault, 2009). For some stationary points with an open-shell singlet ground state, the special strategies need to be considered so as to obtain the stable broken-symmetry solution, which can be found from our previous work (Lv et al., 2019).

2.3. Kinetic calculation

For reactions with the transition state, the transition state theory (Truhlar et al., 1996) was used to calculate the reaction rate constant. In calculation processes, the single-point energies obtained from B2PLYP-D3(BJ)/Def2TZVP level were used as the electronic energies and the partition functions were based on B3LYP-D3(BJ)/6–311++g(d, p) level. The Wigner tunneling transmission was considered in the calculations. For some unimolecular reaction processes, their rate constants may not reach the high-pressure limit in the atmospheric conditions. Thus, RRKM calculations were performed to obtain the relation of rate

constants and pressure. The Lennard-Jones parameters were calculated based on the reference (Gilbert and Smith, 1990) and N_2 was selected as the diluent gas. These parameters can be found in the Table S1. All these kinetic calculations were performed using KiSThelP program (Canneaux et al., 2014). For barrierless reactions occurred in the subsequent reaction processes, the simple hard-sphere collision theory was chosen because its use is sufficient for the evaluation of the favorable pathways. The detail method about hard-sphere theory can be seen in Supplementary Material (Text S1). The molecular radiuses were obtained from Multiwfn software (Lu and Chen, 2012).

2.4. Risk assessment

Human and animals may be exposed to FESOH and its degradation products through air inhalation or other pathways. Thus, the risk of these species needs to be assessed. In this work, we used the BCFBAF module in estimation program interface (EPI) suite to consider bioaccumulation potential of these species (EPA, 2012).

3. Results and discussion

3.1. The conformations of FESOH

The linear FESOH has the feature of many conformers, leading us to figure out which one is the most stable before calculating its reaction with OH radicals. Fig. 1 shows the optimized structures of 10 lower energy conformers, the Gibbs free energies compared with the lowest one and the conformational population at 298 K. It is clear from Fig. 1 that FESOH-5 is the most stable conformer. However, FESOH-2 and FESOH-4 can also exist in the atmosphere because their free energies at 298 K are little (0.09 and 0.18 kcal mol^{-1}) higher than FESOH-5. Combining the obtained Gibbs free energies (Table S2) with the assumption of the Boltzmann distribution, conformational populations of FESOH at different temperatures (223–328 K) can be calculated (Table S2). As shown in Fig. 1 and Table S3, populations of FESOH-2, FESOH-4 and FESOH-5 at 298 K are 32.79%, 27.95% and 38.14%, respectively, indicating that all the three conformers are important and their sum (approximately 99%) are predominant in the atmosphere. With the change of temperatures from 223 K to 328 K, the population sum of the three conformers decrease from 99.76% to 98.27% (Table S3). These results demonstrate that the main existence forms of FESOH in the atmosphere are FESOH-2, FESOH-4 and FESOH-5. Thus, ·OH-initiated FESOH reactions in the following calculation are based on the three conformers.

3.2. The initial reaction of FESOH by OH radicals

As shown in Fig. 2, when FESOH-5 reaction with an OH radical, the H-abstraction routes and ·OH-addition + O_2 routes can be found. For H-abstraction routes, there are three reaction sites (α-C, β-C and δ-C) and five pathways (F5-α1, F5-α2, F5-β1, F5-β2 and F5-δ). These H-abstraction pathways have the similar reaction processes: a pre-reactive complex (RC) is firstly formed when FESOH-5 and an OH radical approach each other; and after stepping over a transition state (TS), a post-reactive complex (PC) is produced; finally, an intermediate (IM) and a H_2O molecule can be obtained with the dissociation of PC. For bimolecular reactions in this work, the Gibbs free energy barrier (or Gibbs free energy of activation) are regarded as the Gibbs free energy difference between reactions and the transition state. Thus, their activation free energies are 6.72 kcal mol^{-1} for F5-α1, 5.17 kcal mol^{-1} for F5-α2, 6.87 kcal mol^{-1} for F5-β1, 8.28 kcal mol^{-1} for F5-β2 and 14.95 kcal mol^{-1} for F5-δ pathways, implying that the F5-α2 is the most favorable pathway and the H-abstraction at α-C site of FESOH-5 is easier to happen.

For H-abstraction reactions, their rate constant changes (seen Table S4) within the range of 223 K–328 K can be obtained ($k_{F5\text{-}\alpha1}$: from 4.18×10^{-12} to 2.83×10^{-12}; $k_{F5\text{-}\alpha2}$: from 1.26×10^{-10} to 3.16×10^{-11}; $k_{F5\text{-}\beta1}$: from 7.95×10^{-12} to 1.81×10^{-12}; $k_{F5\text{-}\beta2}$: from 9.26×10^{-14} to 2.92×10^{-13}; $k_{F5\text{-}\delta}$: from 4.35×10^{-19} to 1.76×10^{-17} cm^3 $molecule^{-1}$ s^{-1}). Their rate ratios are equal to their rate constant ratios due to the same reactant. The rate constant of F5-α2 pathway is several-ten times larger than that of F5-α1 and F5-β1 pathway, 2–3 orders of magnitude higher than that of F5-β2 pathway, and 10^6–10^8 time faster than that for F5-δ pathway. Obviously, the initial reaction at δ-C site cannot happen, the F5-β2 pathway has small contribution to the initial reaction, and the F5-α2 pathway is the most favorable one, meaning that the H-abstraction mainly occur α-C and β-C sites of FESOH.

In addition to H-abstraction reactions, OH radicals can also be added to the S atom of FESOH to form a complex. It is interesting that the

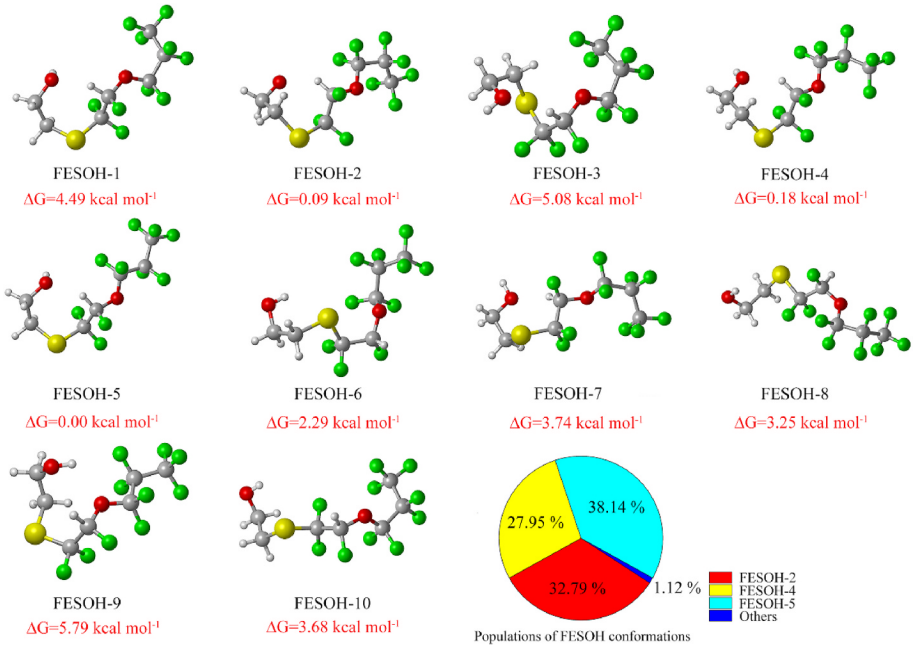

Fig. 1. The optimized structures of 10 lower energy conformers, the related Gibbs free energies with the lowest one and the conformational population at 298 K. The free energy used in the figure and following figures are based on 298 K and 1.01325 bar (1 atm).

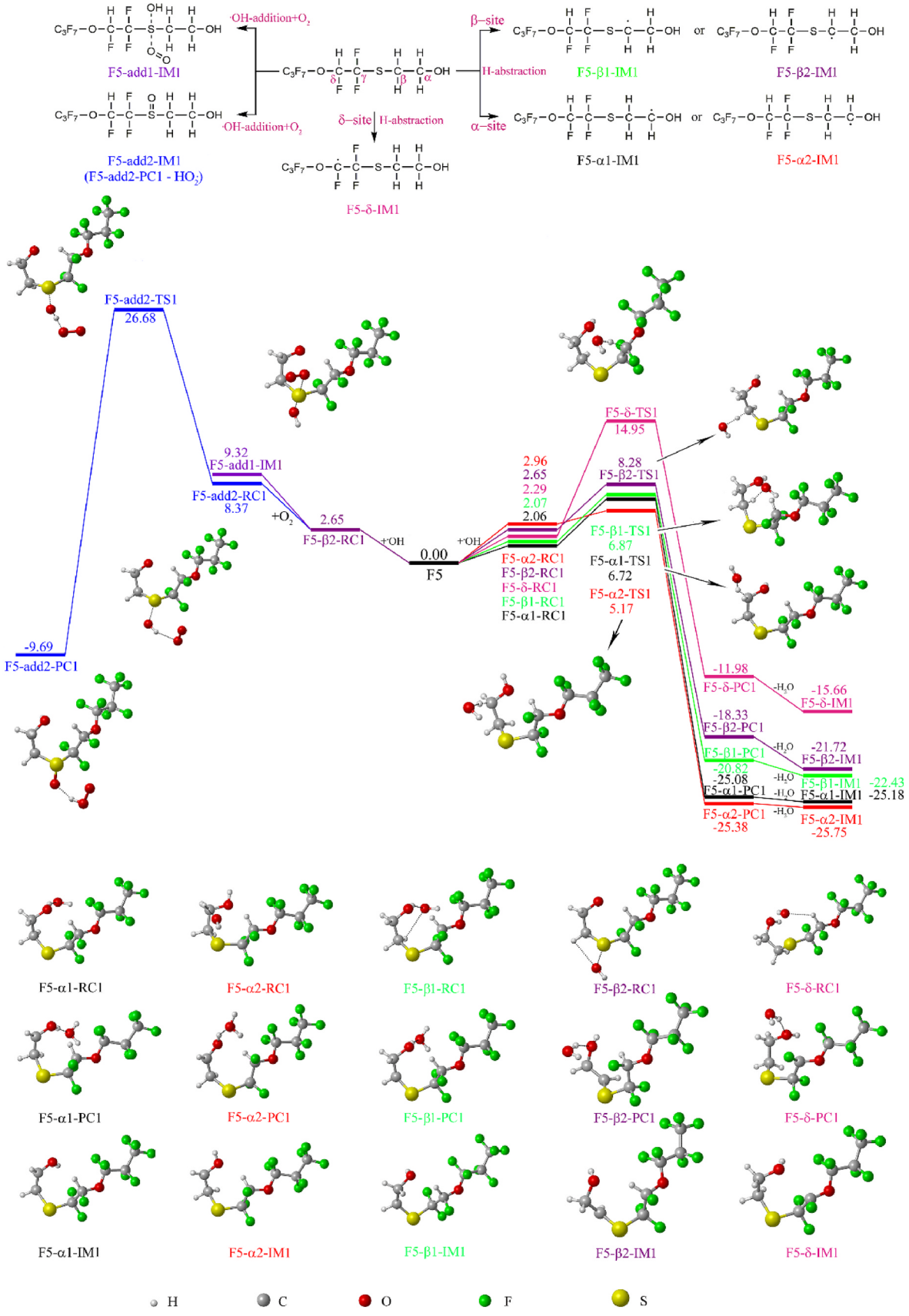

Fig. 2. The scheme of ·OH-initiated FESOH-5 reactions and the corresponding Gibbs free energy profile with the stationary point structures.

addition complex is the same as a RC (F5-β2-RC1) in the H-abstraction reactions. After the complex formation, it can continue reaction with an O_2 molecule via two pathways (F5-add1 and F5-add2). When the O_2 molecule attack the other side of S atom, F5-add1-IM1 can be formed with the free energy increase of 6.67 kcal mol^{-1}. For F5-add1, considering the product in F5-add1 pathway is a complex (F5-add1-IM1), it can be assumed that the complex (F5-add1-IM1) is in equilibrium with O_2 and F5-β2-RC1. Its equilibrium constant is within the range of 4.82 × 10^{-4} to 4.78 × 10^{-6} when the temperature increases from 223 K to 328 K (see Table S4). The result shows that the F5-add1-IM1 cannot occur after reaction equilibrium. In other word, this pathway (F5-add1) is not important. The O_2 molecule can also abstract the H atom of F5-β2-RC1, and the activation free energy of the pathway is 24.03 kcal mol^{-1}, which is obviously higher than the value (5.63 kcal mol^{-1}) corresponding to unimolecular process (F5-β2-RC1 → F5-β2-IM1) in the H-abstraction pathway. The high activation free energy indicates that F5-add2 pathway cannot occur in the initial reaction processes.

To sum up, FESOH-5 is initiated by OH radicals mainly through H-abstraction reaction and mainly at α-C and β-C sites. Initial reaction rate constants (k_{F5}) are equal to rate constants of H-abstraction reaction at α-C site plus the value at β-C site, and are 1.38 × 10^{-10}–3.66 × 10^{-11} cm^3 $molecule^{-1}$ s^{-1} within the range of 223 K–328 K.

For FESOH-2 and FESOH-4, their initial reaction mechanism and results are similar with that of FESOH-5. The detail discussion about the initial reaction of the two conformers is put into Supplementary Material (Text S2–S3, Figs. S1–S2, and Tables S5–S6). Clearly, rate constants of their initial reaction (k_{F2}: from 6.19 × 10^{-11} to 1.54 × 10^{-11}; k_{F4}: from 5.83 × 10^{-11} to 1.24 × 10^{-11} cm^3 $molecule^{-1}$ s^{-1}) are lower than that of FESOH-5.

After analyzing the initial reaction of three main conformers, we can obtain the total reaction rates of FESOH (v_{total}) as the following equation:

$$\begin{aligned} v_{total} &\approx v_{F2} + v_{F4} + v_{F5} \\ &= k_{F2}[\text{FESOH}-2] + k_{F4}[\text{FESOH}-4] + k_{F5}[\text{FESOH}-5] \\ &= k_{F2}p'_{F2}[\text{FESOH}] + k_{F4}p'_{F4}[\text{FESOH}] + k_{F5}p'_{F5}[\text{FESOH}] \\ &= k_{F2,eff}[\text{FESOH}] + k_{F4,eff}[\text{FESOH}] + k_{F5,eff}[\text{FESOH}] = k_{total}[\text{FESOH}] \end{aligned}$$

Where v_{F2}, v_{F4} and v_{F5} are initial reaction rates of FESOH-2, FESOH-4 and FESOH-5, respectively; $k_{F2,eff}$, $k_{F4,eff}$, $k_{F5,eff}$ are called as the effective rate constants for FESOH-2, FESOH-4 and FESOH-5; k_{total} are total rate constants of FESOH; p'_{F2} p'_{F4} and p'_{F5} are conformational populations based on the three conformers, which is different from the populations discussed above because the former populations are constructed from ten conformers. However, the new populations (p'_{F2} p'_{F4} and p'_{F5}) can be gained through the formulas $p_{F2}/(p_{F2}+p_{F4}+p_{F5})$, $p_{F4}/(p_{F2}+p_{F4}+p_{F5})$ and $p_{F5}/(p_{F2}+p_{F4}+p_{F5})$, respectively. The p_{F2}, p_{F4} and p_{F5} are the conformational populations in the section 3.1.

As shown in Fig. 3(a) and Table S7, the total rate constant of FESOH is down from 9.52 × 10^{-11} to 2.24 × 10^{-11} cm^3 $molecule^{-1}$ s^{-1} within the range of 223 K–328 K. These calculated rate constants are consistent with the experiment results (Joudan et al., 2022), meaning that the selected calculation method in the work is reasonable. Fig. 3(a) also describes that the rate constants decrease with the increase of temperature, indicating that low temperature is beneficial for the FESOH degradation by OH radicals. In addition, the contribution of FESOH-5 to total FESOH degradation is more than 60% at 223 K–328 K and is negatively correlated with temperature (Fig. 3(b)). The result means that the reaction of FESOH-5 with OH radicals is the most important at all these temperatures, but the high temperature will make its contribution smaller and lead other conformers (FESOH-2 and FESOH-4) to play bigger role in FESOH degradation. The initial reaction occurred at α-C site (see Fig. 3(b)) accounts for over 80% of the total reaction at 223 K–328 K (k_α/k_{total}), and thus is more important in the oxidation of FESOH by OH radicals.

3.3. The subsequent reaction

Considering the similarity of the initial reaction mechanism and structures for the three conformers and the biggest contribution of FESOH-5 to the total reactions, we will choose the initial reaction products of FESOH-5 to analyze the subsequent reactions. For each site, one initial product (F5-α2-IM1 at α-C site and F5-β1-IM1 at β-C site) is used in view of the reaction process similarity at the same sites. The subsequent reaction can be summarized as the following several processes: (1) the transformation of F5-α2-IM1 (or F5-β1-IM1) to 5αβ-IM3 ($C_3F_7OCHFCF_2S\cdot$); (2) the sulfur removal process; (3) the consecutive chain cleavage cycles.

3.3.1. The transformation of F5-α2-IM1

As depicted in Fig. 4, three pathways can be found for continued reactions of F5-α2-IM1. When O_2 approaches F5-α2-IM1, it either abstract an H atom of F5-α2-IM1 to produce P1 with the activation free energy of 22.93 kcal mol^{-1} at 298 K or is barrierlessly added to the α-C atom to form 5α-IM2. It is obvious from the barrier value that the abstraction reaction cannot occur. In addition, F5-α2-IM1 can also break the S–C bond to form 5α-IM3 ($C_3F_7OCHFCF_2S\cdot$, also called as 5αβ-IM3 in the following) and a vinyl alcohol. Due to lower activation free energy (6.03 kcal mol^{-1}) of S–C breaking reaction, it has the potential to compete with the O_2-addtion process. For barrierless O_2-addtion process, we use hard-sphere collision theory to calculate its rate constant, and the obtained value is 3.14 × 10^{-10} cm^3 $molecule^{-1}$ s^{-1} (Table S8).

The rate constant of the S–C breaking reaction is 2.43 × 10^8 s^{-1} at 298 K by means of TST method, and change from 2.15 × 10^8 s^{-1} to 1.59 × 10^4 s^{-1} within the pressure range of 1.01325–10^{-6} bar at 298 K by means of RRKM theory (Table S9). For the atmospheric reaction, it

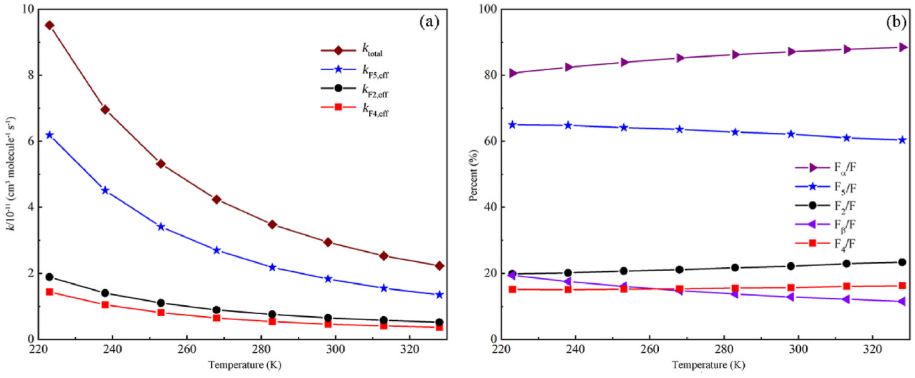

Fig. 3. (a) Total rate constants and effective rate constants of three main conformers (FESOH-2, FESOH-4 and FESOH-5) in initial reactions of FESOH with OH radicals at different temperatures; (b) the contribution of three conformers, α-C site and β-C site of FESOH to total initial reactions at different temperatures.

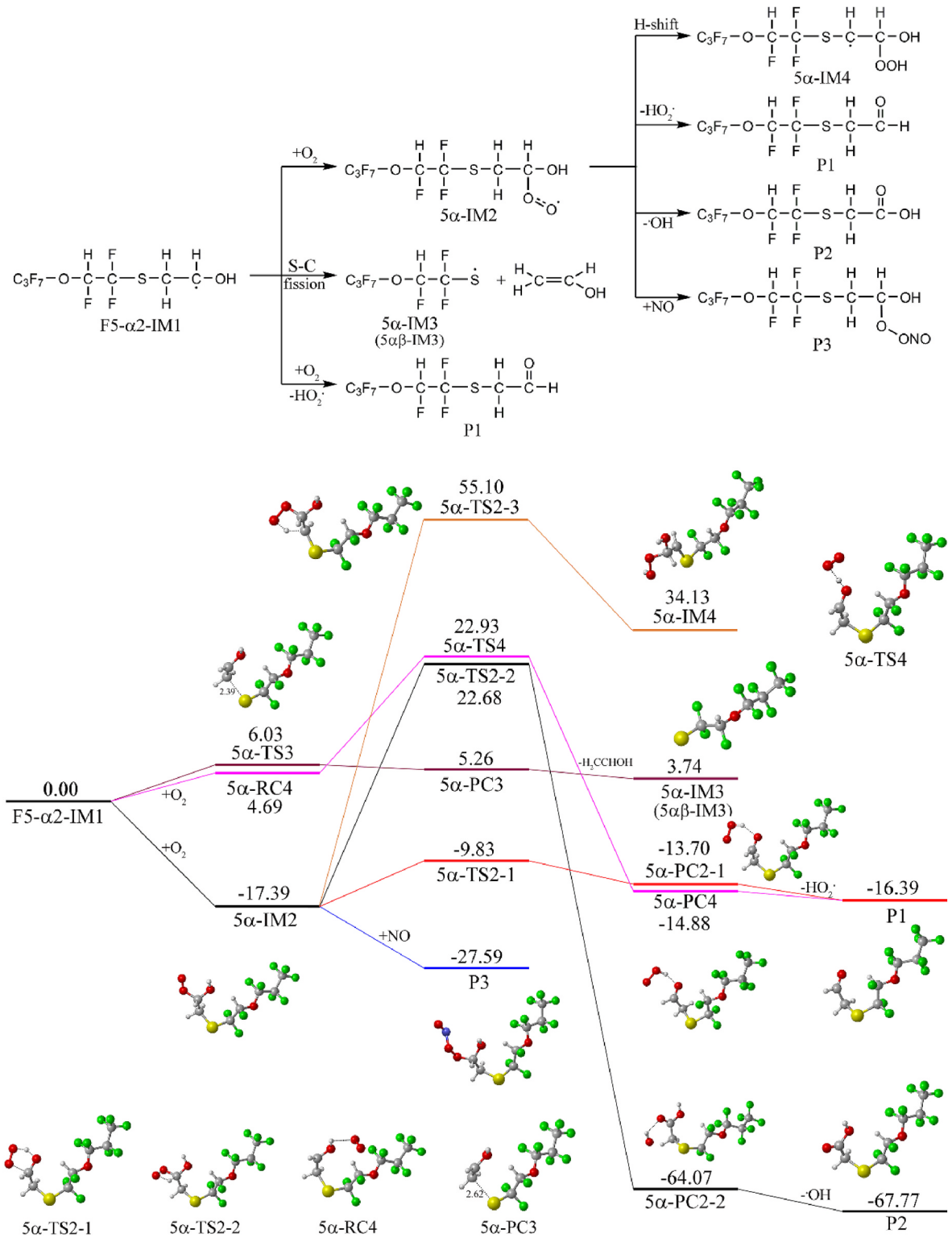

Fig. 4. The subsequent reaction scheme of the initial product F5-α2-IM1 and the corresponding Gibbs free energy profile with the stationary point structures.

mainly occurs in the troposphere. According to the U. S. Standard Atmosphere (NASA and NOAA 1976), we know that the pressure in the troposphere decreases from 1.01325 bar at 0 km to 1.94×10^{-1} bar at 12 km. At the pressure range (1.01325–1.94×10^{-1} bar), the RRKM-based rate constant reduces to 1.66×10^{8} s^{-1} from 2.15×10^{8} s^{-1}, indicating that there is little effect on the rate constant in the pressure range. Using O_2 concentration (5.34×10^{18} molecules cm^{-3} at 0 km obtained from the U. S. Standard Atmosphere (NASA and NOAA 1976)), the rate ratio for the two reactions (O_2 addtion process and S–C breaking) can be written as $v_{O2\text{-addtion}}/v_{S\text{-C breaking}} = (k_{O2\text{-addtion}}[O_2])/k_{S\text{-C breaking}}$. When TST-rate constant of the S–C breaking reaction is used, the value is equal to 6.90. And the value is within the range of 7.80–10.10 if the RRKM-breaking rate constant is used. The results from the different rate calculation methods indicate that two pathways are both important. 5α-IM2, once formed, can be transformed to four different products (5α-IM4, P1, P2 and P3) through intramolecular

H-shift, eliminating HO_2 radical, eliminating OH radical and adding NO molecule. Activation free energies of three unimolecular processes at 298 K are 72.49 kcal mol^{-1} for 5α-IM4 formation, 7.56 kcal mol^{-1} for the P1 formation, 40.07 kcal mol^{-1} for the P2 formation, meaning the P1 formation is the most favorable in the three pathways. The NO addition reaction will form P3, and the reaction is barrierless. To analyze the fate of 5α-IM2, the rate ratio of P1 and P3 formation ($\nu_{P1}/\nu_{P3} = k_{P1}/(k_{P3}[NO])$) need to be calculated. As shown in Tables S8 and S9, $k_{P1\text{-}TST}$ is 3.54×10^7 s^{-1}, $k_{P1\text{-}RRKM}$ is within the range of 1.74×10^7–1.65×10^7 s^{-1} at the pressure range 1.01325–1.94×10^{-1} bar, and k_{P3} is 3.55×10^{-10} cm^3 $molecule^{-1}$ s^{-1}. Thus, whether TST or RRKM method is used, the P1 formation is the most favorable because the rate of this pathway is at least 10^6 times faster than that of P3 formation ([NO] = 0.5 ppbv referenced from U. S. Standard Atmosphere (NASA and NOAA 1976), converting to 1.23×10^{10} molecules cm^{-3} at 1.01325 bar and 298 K). In summary, the initial product F5-α2-IM1 can be directly dissociated to 5αβ-IM3 via S–C bond fission, or is transformed to P1 through adding O_2 and eliminating HO_2 radical processes.

For P1, it can continue to react with other species to finally form 5αβ-IM3 (Fig. 5). The first step is reactions of P1 with OH radicals. When they interact with each other to produce pre-reactive complexes (RC), H-abstraction and ·OH-addition processes can take place, which is described in Fig. 5. The ·OH-addition pathway (path-IM1) occurred at α-C atom has the highest activation free energy (12.10 kcal mol^{-1}) in whole reactions between P1 and radicals, while H-abstraction pathway (path-IM4) at α-C atom has the lowest value (5.40 kcal mol^{-1}). The activation free energies of other H-abstraction process are at middle (P1 + ·OH → 5αP1-IM2 + H_2O, path-IM2: 10.42 kcal mol^{-1}; P1 + ·OH → 5αP1-IM3 + H_2O, path-IM3: 8.35 kcal mol^{-1}; P1 + ·OH → 5αP1-IM3-1 + H_2O, path-IM3-1: 8.33 kcal mol^{-1}). To elucidate the preferable pathway more intuitively, reaction rates of the five pathways are compared. As seen from Table S8, their rate constants at 298 K are 3.81×10^{-16} (k_{IM1}), 1.52×10^{-14} (k_{IM2}), 2.01×10^{-13} (k_{IM3}), 2.67×10^{-13} ($k_{IM3\text{-}1}$), 2.82×10^{-11} (k_{IM4}) cm^3 $molecule^{-1}$ s^{-1}, respectively. Since their reactants are the same, rate ratios are equal to their rate constant ratios. We thus can find that path-IM4 is 10^2–10^5 times faster than other four pathways. In other words, the first product on the transformation processes of P1 to 5αβ-IM3 is the intermediate 5αP1-IM4.

As shown in Fig. 5, 5αP1-IM4 can be degraded to 5αP1-IM6 via two pathways. The one is the barrierless O_2 addition, followed by barrierless NO addition and NO_2 + CO_2 elimination (activation free energy of 22.44 kcal mol^{-1}) processes. The other is the C–C bond cleavage with activation free energy of 9.84 kcal mol^{-1} and reaction free energy of −6.87 kcal mol^{-1}. The high activation free energy of C–C bond cleavage indicates that the barrierless O_2 addition pathways is more likely to occur. It must be said that the ground state of some stationary points in NO_2 elimination processes here and behind involves broken-symmetry. Thus, the special strategy is used to deal with it, and the detail method can be found from our previous work (Lv et al., 2019). The formed 5αP1-IM6 is a radical, and thus can keep reacting with O_2 via the barrierless and spontaneous (reaction free energy of −10.12 kcal mol^{-1}) addition process. The O_2 addition product 5αP1-IM7 can eliminate OH radical to form P5 through the unimolecular process, and can react with NO to produce P6. The reaction with NO is more favorable the than OH radical elimination reaction because it is barrierless and the latter has high activation free energy (44.04 kcal mol^{-1}). Subsequently, NO_2 can be removed from the product P6. The reaction has activation free energy of 22.56 kcal mol^{-1} and reaction free energy of −7.35 kcal mol^{-1}, signifying that NO_2 elimination is not easy to happen and thus P6 can exist in the atmosphere for some time. However, once NO_2 elimination is finished, the formed 5αP1-IM8 is easy to be transformed to 5αP1-IM9 (5αβ-IM3) because of low activation free energy (2.48 kcal mol^{-1}).

3.3.2. The transformation of F5-β1-IM1

Fig. 6 describes all reaction pathways for the F5-β1-IM1 transformation to 5αβ-IM3. After 5β-IM1 formation, the reaction can proceed through three pathways: NO addition, intramolecular H-shift and OH radical elimination. The NO addition reaction is the most favorable because it is barrierless and intramolecular H-shift and OH radical elimination processes have higher activation free energies (67.49 and 40.07 kcal mol^{-1}, respectively). The NO addition product P7 can be converted to 5β-IM2 via a NO_2 elimination process. 5β-IM2 containing an alkoxyl radical group is unstable and can easily take place unimolecular bond fission reaction to form P5 (activation free energy of 1.41 kcal mol^{-1}) or 5β-IM3 (also called as 5αβ-IM3, activation free energy of 0.59 kcal mol^{-1}). An OH radical can abstract the H atom of aldehyde group and –CHF- group of P5, or can be added to C═O bond of aldehyde group of P5. Compared the ·OH-addition of P5 with that of P1 in section 3.3.1, it can be found that the addition and S–C bond fission occur simultaneously for P5. It indicates that S–C bond is less stable than C–C bond when the radical is introduced to the C atom. The H-abstraction of aldehyde group to form 5β-IM5 is the most favorable due to its lowest activation free energy (5.37 kcal mol^{-1}) and fastest rate constant (2.97×10^{-11} cm^3 $molecule^{-1}$ s^{-1}, see in Table S8) in the three pathways at 298 K. 5β-IM5 can undergo two pathways to be transformed to 5αβ-IM3, which is similar with the transformation of 5αP1-IM4. Lower activation free energy (4.73 kcal mol^{-1}) means the CO elimination pathway may have higher contribution to the transformation of 5β-IM5. To prove it, rate ratios of CO elimination process with O_2 addition process are compared ($\nu_{CO\ elimination}/\nu_{5β\text{-}IM6} = k_{CO\ elimination}/(k_{5β\text{-}IM6}[O_2])$). As shown in Table S8 and Table S9, the rate constant of CO elimination at 298 K is 2.17×10^9 s^{-1} by means of TST method, and is within the range of 1.27×10^9–6.37×10^8 s^{-1} at 1.01325–1.94×10^{-1} bar by means of RRKM theory. The O_2 addition rate constant is 2.86×10^{-10} cm^3 $molecule^{-1}$ s^{-1}. Using the O_2 concentration of 5.34×10^{18} molecules cm^{-3}, the rate ratio value is 1.42 or 0.83–0.42, indicating that CO elimination process and O_2 addition process have the similar importance in the transformation of 5β-IM5.

3.3.3. The removal of sulfur

As discussed above, the fate of all initial products at α-C and β-C sites of FESOH-5 is to be degraded to 5αβ-IM3. An O_2 molecule can overcome activation free energy of 12.07 kcal mol^{-1} to be added to 5αβ-IM3 with the formation of 5αβ-IM4 (Fig. 7). -SOO· group of 5αβ-IM4 can rearrange to -S(O·) = O group with activation free energy of 21.77 kcal mol^{-1} (Figs. S3 and S4). It is clear from Figs. S3 and S4 that the rearrangement product is a complex composed of 5αβ-IM5 ($C_3F_7OCHFCF_2$·) and SO_2, and is easy to be dissociated to 5αβ-IM5 and SO_2. 5αβ-IM4 can also react with NO to form P10 barrierlessly, but the reaction free energy of the process is 28.86 kcal mol^{-1}, meaning that the P10 is easy to be transformed back to 5αβ-IM4 and NO. Through a series of processes, P10 will be transformed to 5αβ-IM5 with the production of SO_2 and NO_2. Some high activation free energy processes can be found in the transformation of P10 to 5αβ-IM5. It is clear from the Fig. S3 and the discussion above that the rearrangement reaction of 5αβ-IM4 is more favorable.

3.3.4. The consecutive chain cleavage cycles

After the formation of 5αβ-IM5, the subsequent degradation process will undergo the consecutive chain cleavage cycles (Fig. 7, Figs. S3 and S4). The cycle includes two processes: (1) the transformation of alkyl radical to alkoxyl radical; (2) C–C (or O–C) fission of alkoxyl radical to eliminate a FCOF (or FCOH). The first process can be finished through barrierless O_2 addition, barrierless NO addition and NO_2 elimination of high activation free energy (25.00–28.00 kcal mol^{-1}). The high activation free energy of NO_2 elimination processes in the work is consistent with the same processes in the literature (Huang et al., 2022), indicating that these results is reasonable. The C–C fission of the second process has low activation free energy (<4.00 kcal mol^{-1}), while O–C fission has the higher value (12.73 kcal mol^{-1} for 5αβ-IM10 → 5αβ-IM11). Because an ether group (-O-) exist in main chain, 5αβ-IM11 produced from the second process (5αβ-IM10 → 5αβ-IM11) of the cycle is an alkoxyl radical. Thus, it will directly start the second process of the next cycle to

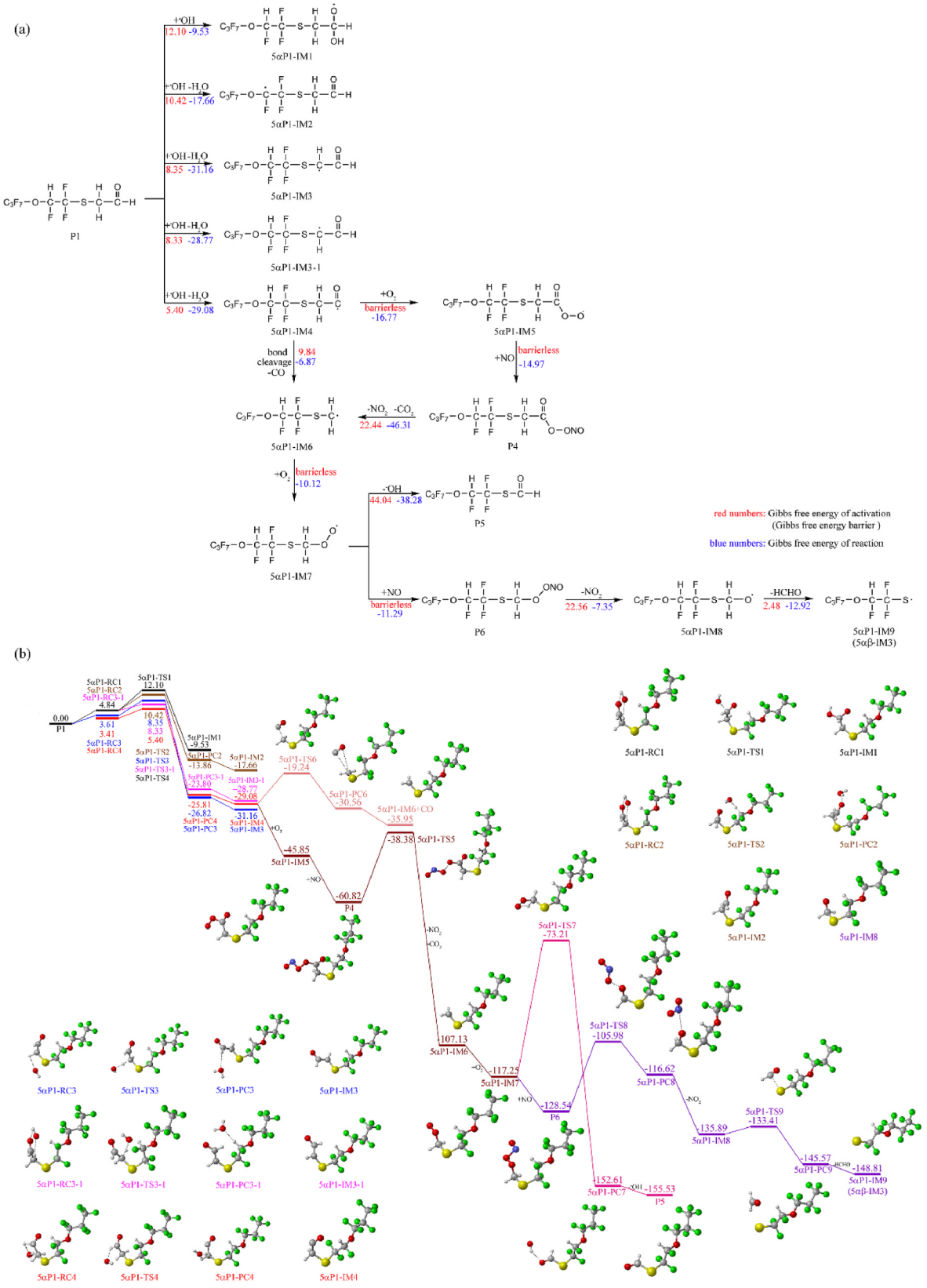

Fig. 5. (a) The transformation process of P1 to 5αβ-IM3 with Gibbs free energies of activation and Gibbs free energies of reactions; (b) the corresponding Gibbs free energy profile with the stationary point structures.

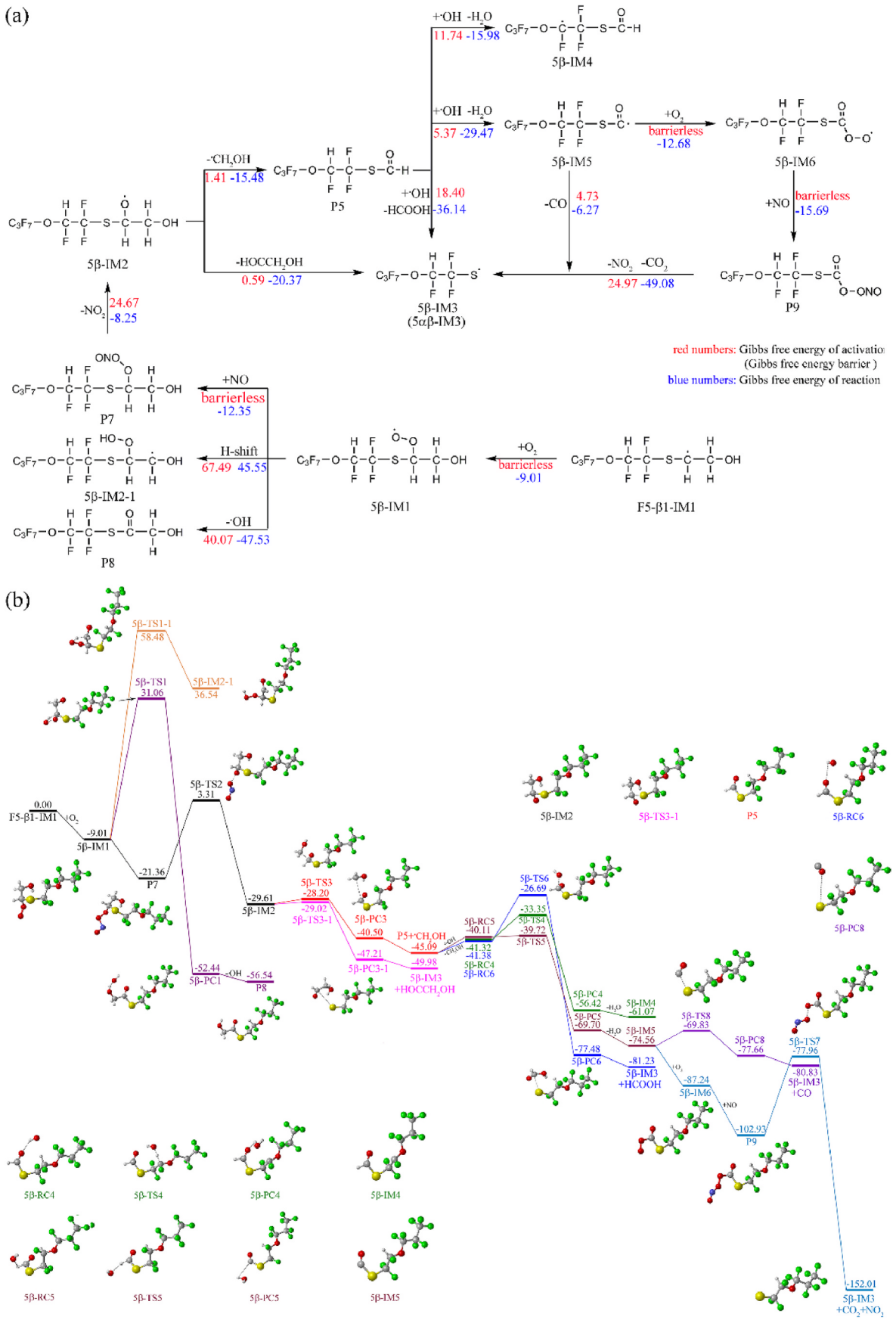

Fig. 6. (a) The subsequent reaction scheme of the initial product (F5-β1-IM1) at β-C site of FESOH with Gibbs free energies of activation and Gibbs free energies of reactions; (b) the corresponding Gibbs free energy profile with the stationary point structures.

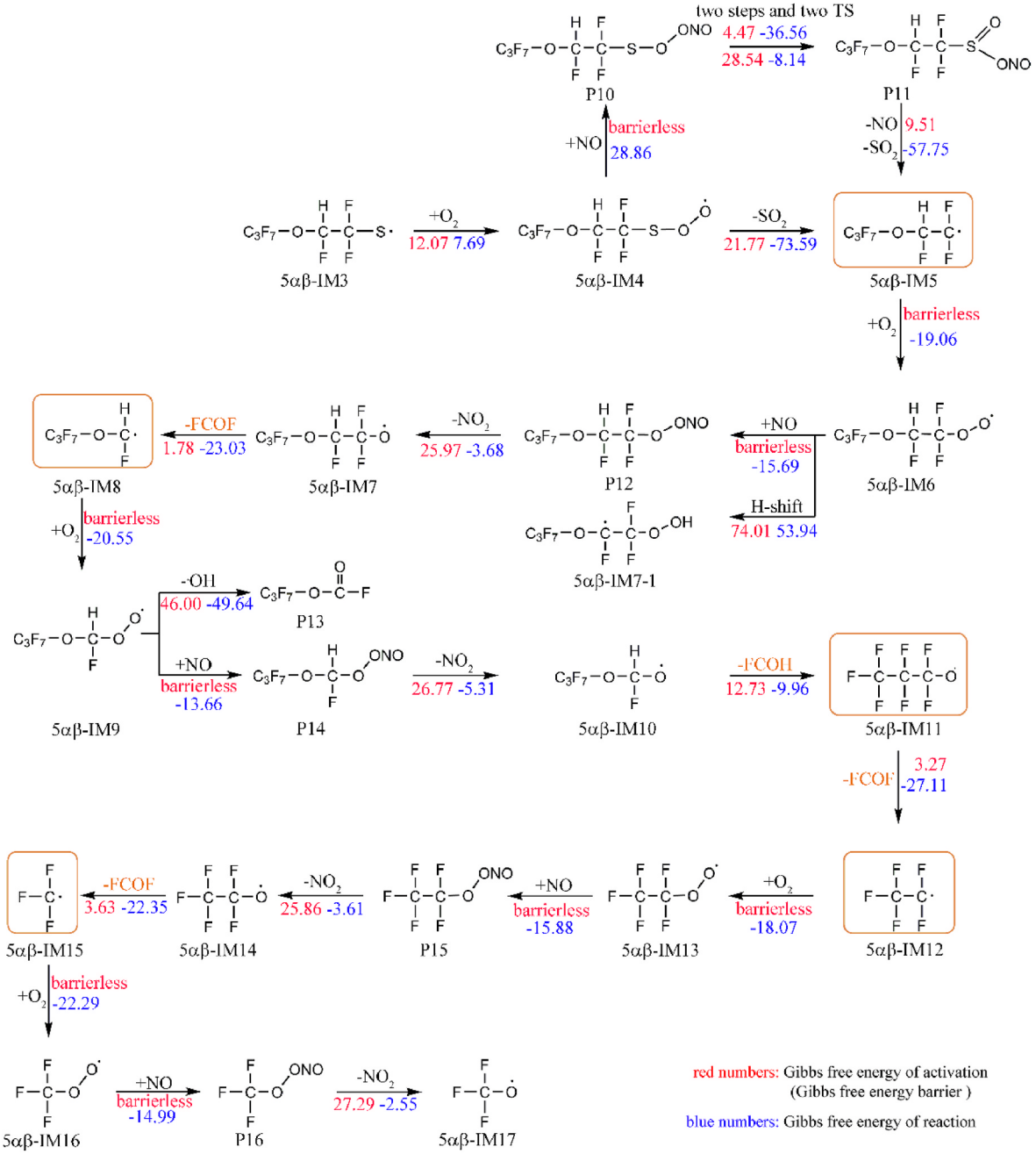

Fig. 7. The scheme of the S-removal and consecutive chain cleavage cycles processes included with Gibbs free energies of activation and Gibbs free energies of reactions.

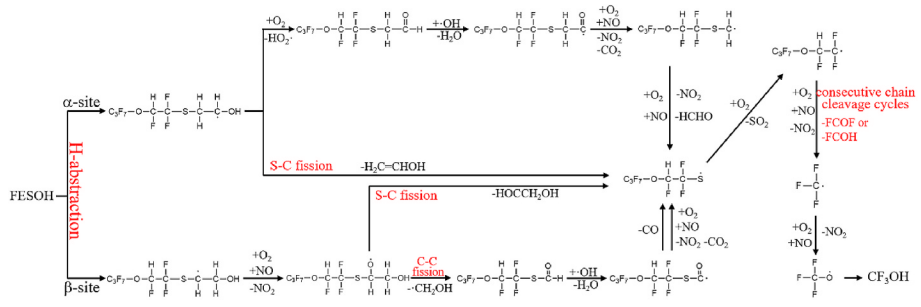

Fig. 8. A reaction scheme of FESOH dominant transformation pathways.

eliminate a FCOF. For 5αβ-IM6, the intramolecular H-shift reaction can also be found, but the reaction process cannot occur because of its high activation free energy (74.01 kcal mol^{-1}). For 5αβ-IM9, it can also take place unimolecular reaction to form P13 and an OH radical with activation free energy of 46.00 kcal mol^{-1}, meaning that the barrierless NO addition is the most favorable pathway. The last formed 5αβ-IM17 can react with an H_2O molecule to form CF_3OH, which can be found from literature (Wallington and Schneider, 1994) and is not discussed in the work.

As discussed above, a complete picture of atmospheric transformation of FESOH in the presence of OH radical, O_2 and NO is displayed. Because many different reaction types and pathways can exist in the FESOH transformation processes, it may be hard to grasp the main results. To facilitate the understanding of FESOH transformation mechanism, a reaction scheme (Fig. 8) including the dominant pathways is drawn.

3.4. Atmospheric implications

Atmospheric transformation of PFASs, especially fluorinated alcohol, has attracted lots of attention. The transformation mechanism studies on the new fluorinated alcohol (FESOH) in the atmosphere provides evidence that the OH radical addition at S atom cannot happen, which can give some guidance for the degradation mechanism studies on species containing the similar groups. No occurrence of PFCAs in the presence of NO also provide more data at molecular level to support the points of literatures (Sulbaek Andersen et al., 2005) that fluorotelomer alcohols cannot be transformed to PFCAs when NO_x exists.

In addition, the analysis above shows a series of NO addition product (R–OONO, alkyl peroxynitrite) need to overcome high activation free energies (>20 kcal mol^{-1}) at 298 K to eliminate NO_2 and form alkyl radicals. Thus, these alkyl peroxynitrite can exist in the atmosphere for some time. To analyze the bioaccumulation potential of FESOH and its transformation products including alkyl peroxynitrite, fluorinated aldehyde and CF_3OH, their bioaccumulation factors (BAF) and bioconcentration factors (BCF) were calculated (Table S10). The BAF/BCF values of all these species from Table S10 are less than 1000 L kg^{-1}, meaning that FESOH and its atmospheric degradation products are not bioaccumulative (Conder et al., 2008).

4. Conclusions

In this work, the theoretical calculation was used to analyze the degradation mechanism of FESOH in the presence of OH radical, O_2 and NO in the atmosphere. The study firstly finds that FESOH has three main conformers (called as FESOH-2, FESOH-4 and FESOH-5). In ·OH-initiated reaction, H atom abstraction processes at α-C and β-C sites of FESOH are preferable to happen because their lower activation free energies (<10 kcal mol^{-1} at 298 K). The kinetics results of initial reactions show that the degradation rate constants of FESOH are within the range of 2.24×10^{-11}–9.52×10^{-11} cm^3 $molecule^{-1}$ s^{-1} at 223–328 K. In addition, it can be concluded from the kinetics analysis that the contribution of FESOH-5 to whole FESOH degradation is more than 60%, and the reaction occur at α-C site exceeds 80%. The initial products at α-C and β-C site can undergo a series of processes to form the same intermediate ($C_3F_7OCHFCF_2S$·). Interacting with O_2, the intermediate can remove S atom to form SO_2 and $C_3F_7OCHFCF_2$·. After consecutive chain cleavage cycles, $C_3F_7OCHFCF_2$· will be transformed to CF_3O·, which can react with H_2O to form CF_3OH. In presence of OH radicals, O_2 and NO, FESOH and its transformation products are not bioaccumulative for human and animals. The mechanism study can not only give us a complete view for ·OH-initial FESOH degradation processes, but also give some insight into the atmospheric fate of other fluorinated alcohols.

CRediT authorship contribution statement

Guochun Lv: Conceptualization, Methodology, Software, Formal analysis, Investigation, Visualization, Writing – original draft, Writing – review & editing. **Jiaoxue Yang:** Software, Formal analysis, Writing – review & editing. **Xiaomin Sun:** Conceptualization, Methodology, Validation, Resources, Project administration, Funding acquisition, Supervision, Writing – review & editing. **Guiyin Wang:** Formal analysis, Visualization, Writing – review & editing. **Zhang Cheng:** Writing – review & editing, Funding acquisition. **Zhanbiao Yang:** Visualization, Writing – review & editing. **Changlian Xu:** Validation, Resources, Writing – review & editing. **Junzhuo Cai:** Validation, Visualization, Writing – review & editing. **Xiaoxun Xu:** Conceptualization, Methodology, Funding acquisition, Supervision, Writing – review & editing.

Declaration of competing interest

The authors declare that they have no known competing financial interests or personal relationships that could have appeared to influence the work reported in this paper.

Data availability

Data will be made available on request.

Acknowledgements

This work is supported by National Natural Science Foundation of China (21976109), Natural Science Foundation of Sichuan Province (2022NSFSC0237, 2021YFN0018).

Appendix A. Supplementary data

Supplementary data to this article can be found online at https://doi.org/10.1016/j.atmosenv.2023.119903.

References

Becke, A.D., 1993. Density-functional thermochemistry. III. The role of exact exchange. J. Chem. Phys. 98, 5648–5652. https://doi.org/10.1063/1.464913.

Canneaux, S., Bohr, F., Henon, E., 2014. KiSThelP: a program to predict thermodynamic properties and rate constants from quantum chemistry results. J. Comput. Chem. 35, 82–93. https://doi.org/10.1002/jcc.23470.

Chen, S., Jiao, X.-C., Gai, N., Li, X.-J., Wang, X.-C., Lu, G.-H., Piao, H.-T., Rao, Z., Yang, Y.-L., 2016. Perfluorinated compounds in soil, surface water, and groundwater from rural areas in eastern China. Environ. Pollut. 211, 124–131. https://doi.org/10.1016/j.envpol.2015.12.024.

Conder, J.M., Hoke, R.A., Wolf, W.d., Russell, M.H., Buck, R.C., 2008. Are PFCAs bioaccumulative? A critical review and comparison with regulatory criteria and persistent lipophilic compounds. Environ. Sci. Technol. 42, 995–1003. https://doi.org/10.1021/es070895g.

Dickman, R.A., Aga, D.S., 2022. A review of recent studies on toxicity, sequestration, and degradation of per- and polyfluoroalkyl substances (PFAS). J. Hazard Mater. 436, 129120 https://doi.org/10.1016/j.jhazmat.2022.129120.

Dreyer, A., Weinberg, I., Temme, C., Ebinghaus, R., 2009. Polyfluorinated compounds in the atmosphere of the atlantic and southern oceans: evidence for a global distribution. Environ. Sci. Technol. 43, 6507–6514. https://doi.org/10.1021/es9010465.

Ellis, D.A., Martin, J.W., De Silva, A.O., Mabury, S.A., Hurley, M.D., Sulbaek Andersen, M.P., Wallington, T.J., 2004. Degradation of fluorotelomer alcohols: a likely atmospheric source of perfluorinated carboxylic acids. Environ. Sci. Technol. 38, 3316–3321. https://doi.org/10.1021/es049860w.

Ellis, D.A., Martin, J.W., Mabury, S.A., Hurley, M.D., Sulbaek Andersen, M.P., Wallington, T.J., 2003. Atmospheric lifetime of fluorotelomer alcohols. Environ. Sci. Technol. 37, 3816–3820. https://doi.org/10.1021/es034136j.

EPA, U., 2012. Estimation Programs Interface Suite™ for Microsoft® Windows, 4.11 citeulike-article-id:9096580.

Folkerson, A.P., Joudan, S., Mabury, S.A., D'eon, J.C., 2021. In vivo transformation of a novel polyfluoroether surfactant. Environ. Toxicol. Chem. 40, 3328–3336. https://doi.org/10.1002/etc.5230.

Frisch, M.J., Trucks, G.W., Schlegel, H.B., Scuseria, G.E., Robb, M.A., Cheeseman, J.R., Scalmani, G., Barone, V., Mennucci, B., Petersson, G.A., Nakatsuji, H., Caricato, M., Li, X., Hratchian, H.P., Izmaylov, A.F., Bloino, J., Zheng, G., Sonnenberg, J.L., Hada, M., Ehara, M., Toyota, K., Fukuda, R., Hasegawa, J., Ishida, M., Nakajima, T.,

Honda, Y., Kitao, O., Nakai, H., Vreven, T., Montgomery, J.A., Peralta, J.E., Ogliaro, F., Bearpark, M., Heyd, J.J., Brothers, E., Kudin, K.N., Staroverov, V.N., Kobayashi, R., Normand, J., Raghavachari, K., Rendell, A., Burant, J.C., Iyengar, S. S., Tomasi, J., Cossi, M., Rega, N., Millam, J.M., Klene, M., Knox, J.E., Cross, J.B., Bakken, V., Adamo, C., Jaramillo, J., Gomperts, R., Stratmann, R.E., Yazyev, O., Austin, A.J., Cammi, R., Pomelli, C., Ochterski, J.W., Martin, R.L., Morokuma, K., Zakrzewski, V.G., Voth, G.A., Salvador, P., Dannenberg, J.J., Dapprich, S., Daniels, A.D., Farkas, Foresman, J.B., Ortiz, J.V., Cioslowski, J., Fox, D.J., 2016. Gaussian 16, Revision C.01.

Fukui, K., 1981. The path of chemical reactions - the IRC approach. Acc. Chem. Res. 14, 363–368. https://doi.org/10.1021/ar00072a001.

Gilbert, R.G., Smith, S.C., 1990. Theory of Unimolecular and Recombination Reactions. Blackwell Scientific Publications, Boston, MA.

Glüge, J., Scheringer, M., Cousins, I.T., DeWitt, J.C., Goldenman, G., Herzke, D., Lohmann, R., Ng, C.A., Trier, X., Wang, Z., 2020. An overview of the uses of per- and polyfluoroalkyl substances (PFAS). Environ. Sci. Proc. Imp. 22, 2345–2373. https://doi.org/10.1039/D0EM00291G.

Grimme, S., 2006. Semiempirical hybrid density functional with perturbative second-order correlation. J. Chem. Phys. 124, 034108 https://doi.org/10.1063/1.2148954.

Grimme, S., Ehrlich, S., Goerigk, L., 2011. Effect of the damping function in dispersion corrected density functional theory. J. Comput. Chem. 32, 1456–1465. https://doi.org/10.1002/jcc.21759.

Harrad, S., de Wit, C.A., Abdallah, M.A.-E., Bergh, C., Björklund, J.A., Covaci, A., Darnerud, P.O., de Boer, J., Diamond, M., Huber, S., Leonards, P., Mandalakis, M., Östman, C., Haug, L.S., Thomsen, C., Webster, T.F., 2010. Indoor contamination with hexabromocyclododecanes, polybrominated diphenyl ethers, and perfluoroalkyl compounds: an important exposure pathway for people? Environ. Sci. Technol. 44, 3221–3231. https://doi.org/10.1021/es903476t.

Hratchian, H.P., Schlegel, H.B., 2004. Accurate reaction paths using a Hessian based predictor–corrector integrator. J. Chem. Phys. 120, 9918–9924. https://doi.org/10.1063/1.1724823.

Hratchian, H.P., Schlegel, H.B., 2005. Using hessian updating to increase the efficiency of a hessian based predictor-corrector reaction path following method. J. Chem. Theor. Comput. 1, 61–69. https://doi.org/10.1021/ct0499783.

Huang, Y., Zhang, X., Li, C., Zhao, Y., Zhang, Y.-n., Qu, J., 2022. Atmospheric persistence and toxicity evolution for fluorinated biphenylethyne liquid crystal monomers unveiled by in silico methods. J. Hazard Mater. 424, 127519 https://doi.org/10.1016/j.jhazmat.2021.127519.

Joudan, S., Mabury, S.A., 2022. Aerobic biotransformation of a novel highly functionalized polyfluoroether-based surfactant using activated sludge from a wastewater treatment plant. Environ. Sci. Proc. Imp. 24, 62–71. https://doi.org/10.1039/D1EM00358E.

Joudan, S., Orlando, J.J., Tyndall, G.S., Furlani, T.C., Young, C.J., Mabury, S.A., 2022. Atmospheric fate of a new polyfluoroalkyl building block, C3F7OCHFCF2SCH2CH2OH. Environ. Sci. Technol. 56, 6027–6035. https://doi.org/10.1021/acs.est.0c07584.

Krishnan, R., Binkley, J.S., Seeger, R., Pople, J.A., 1980. Self-consistent molecular orbital methods. XX. A basis set for correlated wave functions. J. Chem. Phys. 72, 650–654. https://doi.org/10.1063/1.438955.

Legault, C.Y., 2009. CYLview, 1.0b, université de Sherbrooke. http://www.cylview.org.

Li, J., Sun, J., Li, P., 2022. Exposure routes, bioaccumulation and toxic effects of per- and polyfluoroalkyl substances (PFASs) on plants: a critical review. Environ. Int. 158, 106891 https://doi.org/10.1016/j.envint.2021.106891.

Liu, S., Yin, N., Faiola, F., 2018. PFOA and PFOS disrupt the generation of human pancreatic progenitor cells. Environ. Sci. Technol. Lett. 5, 237–242. https://doi.org/10.1021/acs.estlett.8b00193.

Lohmann, R., Cousins, I.T., DeWitt, J.C., Glüge, J., Goldenman, G., Herzke, D., Lindstrom, A.B., Miller, M.F., Ng, C.A., Patton, S., Scheringer, M., Trier, X., Wang, Z., 2020. Are fluoropolymers really of low concern for human and environmental health and separate from other PFAS? Environ. Sci. Technol. 54, 12820–12828. https://doi.org/10.1021/acs.est.0c03244.

Lu, T., 2021. Molclus Program, Version 1.9.9.5. http://www.keinsci.com/research/molclus.html.

Lu, T., Chen, F., 2012. Multiwfn: a multifunctional wavefunction analyzer. J. Comput. Chem. 33, 580–592. https://doi.org/10.1002/jcc.22885.

Lv, G., Sun, X., 2021. The molecular-level understanding of the uptake of PFOS and its alternatives (6:2 Cl-PFESA and OBS) into phospholipid bilayers. J. Hazard Mater. 417, 125991 https://doi.org/10.1016/j.jhazmat.2021.125991.

Lv, G., Zhang, C., Sun, X., 2019. Understanding the oxidation mechanism of methanesulfinic acid by ozone in the atmosphere. Sci. Rep. 9, 322. https://doi.org/10.1038/s41598-018-36405-0.

McLean, A.D., Chandler, G.S., 1980. Contracted Gaussian basis sets for molecular calculations. I. Second row atoms, Z=11–18. J. Chem. Phys. 72, 5639–5648. https://doi.org/10.1063/1.438980.

NASA, NOAA, 1976. U.S. Standard Atmosphere.

O'Boyle, N.M., Banck, M., James, C.A., Morley, C., Vandermeersch, T., Hutchison, G.R., 2011a. Open Babel: an open chemical toolbox. J. Cheminf. 3, 33. https://doi.org/10.1186/1758-2946-3-33.

O'Boyle, N.M., Vandermeersch, T., Flynn, C.J., Maguire, A.R., Hutchison, G.R., 2011b. Confab - systematic generation of diverse low-energy conformers. J. Cheminf. 3, 8. https://doi.org/10.1186/1758-2946-3-8.

Podder, A., Sadmani, A.H.M.A., Reinhart, D., Chang, N.-B., Goel, R., 2021. Per and poly-fluoroalkyl substances (PFAS) as a contaminant of emerging concern in surface water: a transboundary review of their occurrences and toxicity effects. J. Hazard Mater. 419, 126361 https://doi.org/10.1016/j.jhazmat.2021.126361.

Stewart, J.J.P., 2013. Optimization of parameters for semiempirical methods VI: more modifications to the NDDO approximations and re-optimization of parameters. J. Mol. Model. 19, 1–32. https://doi.org/10.1007/s00894-012-1667-x.

Stewart, J.J.P., 2016. MOPAC2016.

Styler, S.A., Myers, A.L., Donaldson, D.J., 2013. Heterogeneous photooxidation of fluorotelomer alcohols: a new source of aerosol-phase perfluorinated carboxylic acids. Environ. Sci. Technol. 47, 6358–6367. https://doi.org/10.1021/es4011509.

Sulbaek Andersen, M.P., Nielsen, O.J., Hurley, M.D., Ball, J.C., Wallington, T.J., Ellis, D. A., Martin, J.W., Mabury, S.A., 2005. Atmospheric chemistry of 4:2 fluorotelomer alcohol (n-C4F9CH2CH2OH): products and mechanism of Cl atom initiated oxidation in the presence of NOx. J. Phys. Chem. 109, 1849–1856. https://doi.org/10.1021/jp045672g.

Tansel, B., 2022. PFAS use in electronic products and exposure risks during handling and processing of e-waste: a review. J. Environ. Manag. 316, 115291 https://doi.org/10.1016/j.jenvman.2022.115291.

Thackray, C.P., Selin, N.E., 2017. Uncertainty and variability in atmospheric formation of PFCAs from fluorotelomer precursors. Atmos. Chem. Phys. 17, 4585–4597. https://doi.org/10.5194/acp-17-4585-2017.

Thackray, C.P., Selin, N.E., Young, C.J., 2020. A global atmospheric chemistry model for the fate and transport of PFCAs and their precursors. Environ. Sci. Proc. Imp. 22, 285–293. https://doi.org/10.1039/C9EM00326F.

Truhlar, D.G., Garrett, B.C., Klippenstein, S.J., 1996. Current status of transition-state theory. J. Phys. Chem. 100, 12771–12800. https://doi.org/10.1021/jp953748q.

Wallington, T.J., Hurley, M.D., Xia, J., Wuebbles, D.J., Sillman, S., Ito, A., Penner, J.E., Ellis, D.A., Martin, J., Mabury, S.A., Nielsen, O.J., Sulbaek Andersen, M.P., 2006. Formation of C7F15COOH (PFOA) and other perfluorocarboxylic acids during the atmospheric oxidation of 8:2 fluorotelomer alcohol. Environ. Sci. Technol. 40, 924–930. https://doi.org/10.1021/es051858x.

Wallington, T.J., Schneider, W.F., 1994. The stratospheric fate of CF3OH. Environ. Sci. Technol. 28, 1198–1200. https://doi.org/10.1021/es00055a036.

Wang, Q., Ruan, Y., Lin, H., Lam, P.K.S., 2020. Review on perfluoroalkyl and polyfluoroalkyl substances (PFASs) in the Chinese atmospheric environment. Sci. Total Environ. 737, 139804 https://doi.org/10.1016/j.scitotenv.2020.139804.

Wang, S., Huang, J., Yang, Y., Hui, Y., Ge, Y., Larssen, T., Yu, G., Deng, S., Wang, B., Harman, C., 2013. First report of a Chinese PFOS alternative overlooked for 30 Years: its toxicity, persistence, and presence in the environment. Environ. Sci. Technol. 47, 10163–10170. https://doi.org/10.1021/es401525n.

Wang, Z., DeWitt, J.C., Higgins, C.P., Cousins, I.T., 2017. A never-ending story of per- and polyfluoroalkyl substances (PFASs)? Environ. Sci. Technol. 51, 2508–2518. https://doi.org/10.1021/acs.est.6b04806.

Weigend, F., 2006. Accurate Coulomb-fitting basis sets for H to Rn. Phys. Chem. Chem. Phys. 8, 1057–1065. https://doi.org/10.1039/B515623H.

Weigend, F., Ahlrichs, R., 2005. Balanced basis sets of split valence, triple zeta valence and quadruple zeta valence quality for H to Rn: design and assessment of accuracy. Phys. Chem. Chem. Phys. 7, 3297–3305. https://doi.org/10.1039/B508541A.

Yao, Y., Chang, S., Zhao, Y., Tang, J., Sun, H., Xie, Z., 2017. Per- and poly-fluoroalkyl substances (PFASs) in the urban, industrial, and background atmosphere of Northeastern China coast around the Bohai Sea: occurrence, partitioning, and seasonal variation. Atmos. Environ. 167, 150–158. https://doi.org/10.1016/j.atmosenv.2017.08.023.

Yao, Y., Sun, H., Gan, Z., Hu, H., Zhao, Y., Chang, S., Zhou, Q., 2016. Nationwide distribution of per- and polyfluoroalkyl substances in outdoor dust in mainland China from eastern to western areas. Environ. Sci. Technol. 50, 3676–3685. https://doi.org/10.1021/acs.est.6b00649.

Yarwood, G., Kemball-Cook, S., Keinath, M., Waterland, R.L., Korzeniowski, S.H., Buck, R.C., Russell, M.H., Washburn, S.T., 2007. High-resolution atmospheric modeling of fluorotelomer alcohols and perfluorocarboxylic acids in the north American troposphere. Environ. Sci. Technol. 41, 5756–5762. https://doi.org/10.1021/es0708971.

Yu, S., Liu, W., Xu, Y., Zhao, Y., Wang, P., Wang, X., Li, X., Cai, C., Liu, Y., Xiong, G., Tao, S., Liu, W., 2018. Characteristics of perfluoroalkyl acids in atmospheric PM10 from the coastal cities of the Bohai and Yellow Seas, Northern China. Environ. Pollut. 243, 1894–1903. https://doi.org/10.1016/j.envpol.2018.10.002.